

Dynamical dispersal of primordial asteroid families



P.I.O. Brasil^{a,*}, F. Roig^a, D. Nesvorný^b, V. Carruba^c, S. Aljbae^c, M.E. Huaman^c

^aON, Observatório Nacional, COAA, Rio de Janeiro, RJ 20921-400, Brazil

^bSouthwest Research Institute, 1050 Walnut Street, Suite 300, Boulder, CO 80302, United States

^cUNESP, Universidade Estadual Paulista, Grupo de Dinâmica Orbital e Planetologia, Guaratinguetá, SP 12516-410, Brazil

ARTICLE INFO

Article history:

Received 22 July 2015

Revised 7 November 2015

Accepted 16 November 2015

Available online 23 November 2015

Keywords:

Asteroids, dynamics

Planets, migration

Resonances, orbital

ABSTRACT

Many asteroid families are identified and well characterized all over the main asteroid belt. Interestingly, however, none of them are older than 4 Gyr. Many mechanisms have been proposed to disperse such old primordial asteroid families that presumably have existed, but only very few have really worked. Here we present a plausible mechanism for dispersing primordial asteroid families that is based on the 5-planet instability model known as jumping Jupiter. Using two different evolutions for the jumping-Jupiter model, we have numerically integrated orbits of eight putative primordial families. Our results show that the most important effect on the asteroid families' eccentricity and inclination dispersal is that of the secular resonances, in some cases associated with the mean motion resonances. As for the semimajor axes spreading we find that the principal effect is that of close encounters with the fifth giant planet whose orbit briefly overlaps with (part of) the main belt. Therefore, the existence of a fifth giant planet with the mass comparable with that of Uranus' or Neptune's could contribute in important ways to dispersal of the primordial asteroid families. To have that effect, the interloper planet should go into and considerably interact with the asteroids during the instability phase.

© 2015 Elsevier Inc. All rights reserved.

1. Introduction

Asteroid dynamical families are defined as clumps of objects that share similar proper orbital elements. A dynamical family may be constituted by one or more collisional families that formed by catastrophic or cratering impacts on parent bodies (e.g. Milani et al., 2014; Dykhuus and Greenberg, 2015). Up to now, more than 100 asteroid families have been identified (Nesvorný et al., in press; Spoto et al., 2015; Brož et al., 2013). According to Brož et al. (2013), the majority of the families have estimated ages less than 2 Gyr, and their parent bodies diameters are <100 km. Furthermore, Brož et al. (2013) have not found any families that could date to the epoch of the instability associated with the Late Heavy Bombardment, hereafter LHB (Gomes et al., 2005), roughly 4 Gyr ago. This fact seems to be in contradiction with what is expected for a primordial asteroid belt, because many bodies should have been disrupted during the LHB. Thus, Brož et al. (2013) considered many effects that could be responsible for the dispersion of asteroid families during the instability phase and later, such as secondary disruptions of family members by cometary and asteroid impacts, families overlap, dispersion by the Yarkovsky

effect (Bottke et al., 2002), collisional comminution, and dynamical perturbations by migrating planets.

Here we consider the dynamical perturbations by migrating planets. Brož et al. (2013) studied the evolution of four families formed during the LHB in the inner, central and outer main belt ($2.1 < a < 3.2$ AU). In their simulations, planetary orbital elements during the instability were interpolated following a jumping-Jupiter evolution with four giant planets, taken from Morbidelli et al. (2010). They found that the instability phase in the jumping-Jupiter model cannot disperse the inclinations of family members, and in some cases (low eccentricity families) not even their eccentricities. They concluded that families that formed during the LHB would remain clustered, and should be recognizable today. In fact, the authors found that only few mechanisms (e.g. collisional comminution) could explain why the primordial families are not presently found in the asteroid belt. In this work we propose to study the dynamics of hypothetical asteroid families during the instability using a more realistic model of the evolution of the outer planets.

It is now well accepted that the giant planets acquired their current orbits after a period of migration, due to their interaction with a planetesimal disk initially exterior to Neptune's orbit (Fernández and Ip, 1984; Hahn and Malhotra, 1999). Also, since the first version of the Nice model was proposed by Tsiganis et al. (2005),

* Corresponding author.

E-mail address: pedro_brasil87@hotmail.com (P.I.O. Brasil).

Morbidelli et al. (2005), it seems to be likely that, during migration, the planetary system underwent a dynamical instability phase that could explain many characteristics of its current architecture. Such an instability should have also leave fingerprints in the asteroid belt.

Minton and Malhotra (2009), using a simplified model of smooth exponential migration, showed that, as planets migrate, mean motion and secular resonances sweep through the asteroid belt, and might have sculpted its orbital structure. However, the best-fitting migration e-folding rate was found to be ≈ 0.5 Myr, which is too fast in terms of a planetesimal driven migration with a reasonable mass of the outer disk (Tsiganis et al., 2005; Levison et al., 2008; Morbidelli et al., 2010; Nesvorný and Morbidelli, 2012). Additionally, Brassier et al. (2009) argued that Jupiter's semimajor axis displacement must be fast to avoid excitation of the terrestrial planet orbits by secular resonances ($g_1 = g_5$ and $g_2 = g_5$).

On the other hand, Morbidelli et al. (2009) showed that close encounters between the four giant planets are needed in order to explain Jupiter's eccentricity excitation. Thus, Jupiter most likely participated in planetary encounters with Uranus, which make Jupiter's semimajor axis to underwent significant changes on short timescales. This possibility was named the jumping-Jupiter model. Morbidelli et al. (2010) showed that models of smooth planetesimal-driven migration with more reasonable time scales (~ 5 Myr) cannot reproduce the current orbital distribution of the asteroid belt, while the jumping-Jupiter model does.

A more recent development of the jumping-Jupiter model considers that the outer Solar System could have had more than four giant planets. This is because it is found in the simulations that many times an ice giant is ejected from the Solar System after having encounters with Jupiter (Nesvorný, 2011; Nesvorný and Morbidelli, 2012). The initial configuration with five giant planets leads to the instability and migration histories that satisfy many constraints. Following this approach, it is possible to explain the capture of Jupiter's Trojans and irregular satellites (Nesvorný et al., 2013, 2014a), the preservation of the Galilean satellites during the instability phase (Deienno et al., 2014), the formation of the hot Kuiper belt objects (Brasil et al., 2014), and the main structure of the Kuiper belt kernel (Nesvorný, 2015). In this paper we use the evolution of the giant planets given by Nesvorný and Morbidelli (2012) to study the effects of the jumping-Jupiter instability on the structure of the asteroid families that could have formed before the LHB epoch.

The paper is divided as follows. Section 2 describes the methods employed to setup the initial families, the integration algorithm, and the dynamical maps that were used to interpret the results. We present and discuss our results in Section 3, and the conclusions are given in Section 4.

2. Methods

Our main goal is to model the dynamical effects of the jumping-Jupiter instability on asteroid families. First, we consider 8 fictitious families that would represent their behavior in the three regions of the main belt (inner, central, outer), at both high and low inclinations (Fig. 1). Each fictitious family has initially 1000 members whose semimajor axes, eccentricities and inclinations are generated according to the procedure described in Section 2.1. The families we have considered are, in order of increasing semimajor axis: Vesta, Phocaea, Hansa, Koronis, Eos, Themis, and Euphrosyne. We stress that these names have nothing to do with the current families, but only refer to the parent body that is used to generate the fictitious families. The idea is that the generated families represent primordial families that could have existed

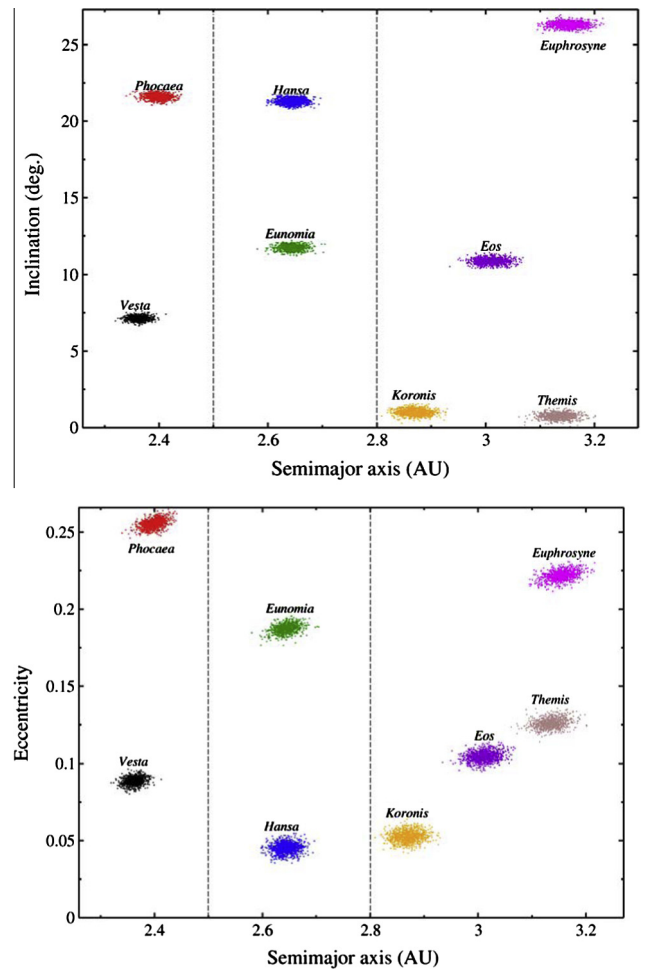


Fig. 1. Initial orbital distribution of synthetic primordial, pre-LHB families. Inclination with semimajor axis (upper panel), and eccentricity with semimajor axis (bottom panel). The color code denotes the fictitious primordial families with locations resembling the real ones: Vesta (black), Phocaea (red), Eunomia (green), Hansa (blue), Koronis (orange), Eos (violet), Themis (brown), and Euphrosyne (magenta). Dashed vertical lines stand for the approximate boundaries of the inner, central, and outer main belt regions. (For interpretation of the references to color in this figure legend, the reader is referred to the web version of this article.)

before the instability phase on similar orbits as some present families.

2.1. The setup of initial families

In order to create the fictitious asteroid families, we apply a very simple model of catastrophic breakup. We assume that the distribution of the ejection velocities of the fragments, $N(v_{ej})$, is a Maxwell distribution with the mean ejection velocity \bar{v}_{ej} , given as input parameter. We also assume that the individual ejection velocity is independent of fragment's mass (e.g. Giblin et al., 1998), and that the ejection velocity field is isotropic with respect to the parent body. The escape velocity from the parent body is estimated as

$$v_{esc}^2 = 1.64 G \frac{4}{3} \pi \rho R^2$$

(Petit and Farinella, 1993), where ρ and R are the density and radius of the parent body, respectively, and G is the gravitational constant. Only fragments with $v_{ej} > v_{esc}$ are able to escape with relative velocity at infinity given by $v_{\infty}^2 = v_{ej}^2 - v_{esc}^2$. From the distribution $N(v_{ej})$, we obtain the correlated distribution $N(v_{\infty})$, applying an

upper cutoff, $v_{\text{cut}} = 600 \text{ ms}^{-1}$. The distribution $N(v_{\infty})$ is then decomposed into the distributions tangential to the orbit, $N(v_T)$, radial, $N(v_R)$, and normal, $N(v_W)$. Finally, the orbital elements a, e, i of each fragment are computed using Gauss equations, while the angles λ, ϖ, Ω , namely the mean longitude, the longitude of the pericenter, and the longitude of the ascending node, are set equal to those of the parent body. To evaluate Gauss equations, we need to assume the values of the true anomaly, f , and the argument of perihelion, ω , of the parent body at the breakup (which are not related to λ, ϖ, Ω). Here, we choose $f = 90^\circ$ and $f + \omega = 0^\circ$ (e.g. Morbidelli et al., 1995). Typical values of \bar{v}_{ej} adopted here vary between 100 and 300 ms^{-1} , which produce very compact initial families. The use of too compact families, although probably unrealistic (e.g. Farinella et al., 1993), provides tighter constraints on the efficiency of the instability to disrupt the families.

2.2. Planetary instability phase

Our simulations are based on the original evolution presented in Nesvorný (2011) and Nesvorný and Morbidelli (2012), in particular the five-planet simulations. These previous studies focused on the several constraints to define the success of their simulations. Namely, the successful evolution should end up with four giant planets with orbits resembling the actual ones. Jupiter's eccentricity must be excited and the separation between Saturn and Jupiter should occur quickly (less than 1 Myr). As mentioned in Section 1, other studies have used these models to analyze the effects of such evolution on the small body populations such as the Galilean satellites (Deianno et al., 2014), Jupiter's Trojans and irregular satellites (Nesvorný et al., 2013, 2014a), the exterior moons of Saturn (Nesvorný et al., 2014b), Kuiper belt objects (Brasil et al., 2014; Nesvorný, 2015), and the asteroid main belt (Roig and Nesvorný, 2015). We apply the same models to understand the consequences for the pre-LHB asteroid families.

We consider two of the three cases used by Nesvorný et al. (2013) and Deianno et al. (2014), namely case_1 and case_3 (see Figs. 16 and 14, respectively, in Nesvorný and Morbidelli (2012)). We have ruled out case_2, because the extra ice planet in this case goes deep inside the asteroid belt and excites too much the asteroids eccentricities (Roig and Nesvorný, 2015). A similar effect is reported by Deianno et al. (2014) for the Galilean satellites. Fig. 2 illustrates the instability phase in cases 1 and 3 in detail, focusing on Jupiter's semimajor axis and the heliocentric distance of the extra ice planet. One notes that in case_3 the extra planet does not penetrate the main belt region ($2.1 < a < 3.2 \text{ AU}$) as deeply as in case_1. Thus, in principle, the effects of case_3 on the asteroid families might not be as strong as in case_1. A more detailed discussion is presented in Section 3.

2.3. Numerical integrations

The simulations are carried out using a modified version of the SWIFT_RMVS3 symplectic integrator.¹ Our modified version of the integrator does not propagate the orbits of the planets. Instead, it reproduces their evolution by reading the positions and velocities from a file that was previously stored with 1-yr spacing. The algorithm performs a two-body like interpolation for the intermediate times (see Nesvorný et al., 2013). The coordinate files for the two migration cases considered here have been recreated from the simulations by Nesvorný (2011) and Nesvorný and Morbidelli (2012).

On the other hand, the test particles are propagated using a classical second order leap-frog scheme, feeling the gravitational perturbation of the major planets. Close encounters between the

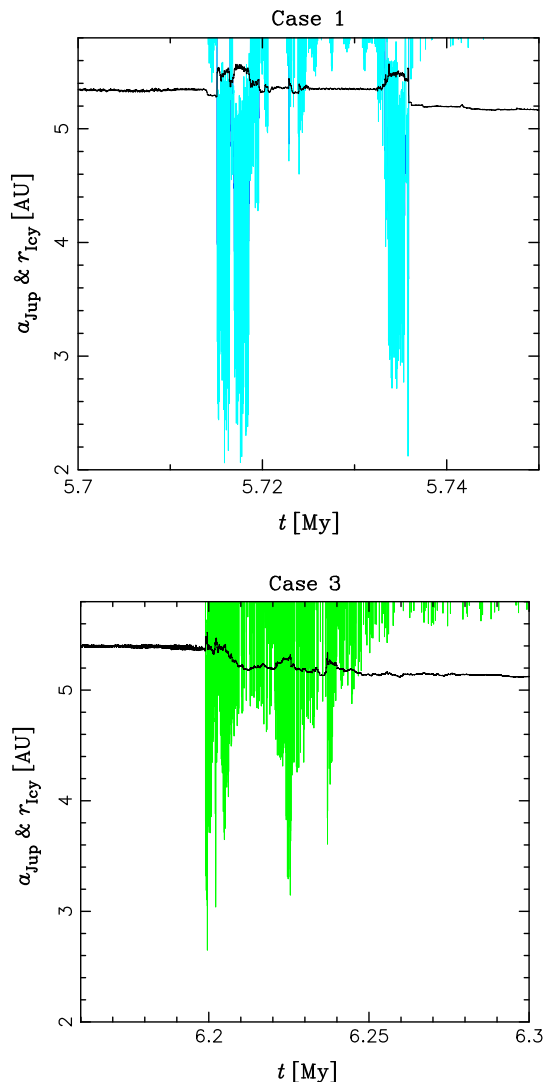


Fig. 2. Temporal evolution of Jupiter's semimajor axis (black) and the fifth (interloper) planet heliocentric distance for cases 1 and 3 (in cyan and green, respectively). It is worth noting that the fifth planet temporarily reaches smaller heliocentric distances in case_1 than in case_3. (For interpretation of the references to color in this figure legend, the reader is referred to the web version of this article.)

test particles and the planets are managed by the RMVS3 routines. The total simulation timespan is 10 Myr. The integration time step is 0.05 yr.

We have modified the code to also register in a separate file the positions and velocities of any test particle during each close encounter within three Hill's radii to any planet. In this way, by comparing the position and velocity at the beginning and at the end of an encounter, we can determine the net change in the heliocentric orbital elements of the particle that is produced by that encounter.

2.4. Dynamical maps

To help in the interpretation of the asteroid dynamics occurring in the jumping-Jupiter model, we construct dynamical maps for three different families, Vesta, Eunomia and Koronis, at two times corresponding to different planetary configurations. Here we only present the analysis of the maps for case_1 at $t = 0$ (beginning of the simulation) and at $t = 10 \text{ Myr}$ (end of the simulation). The

¹ <https://www.boulder.swri.edu/hal/swift.html>.

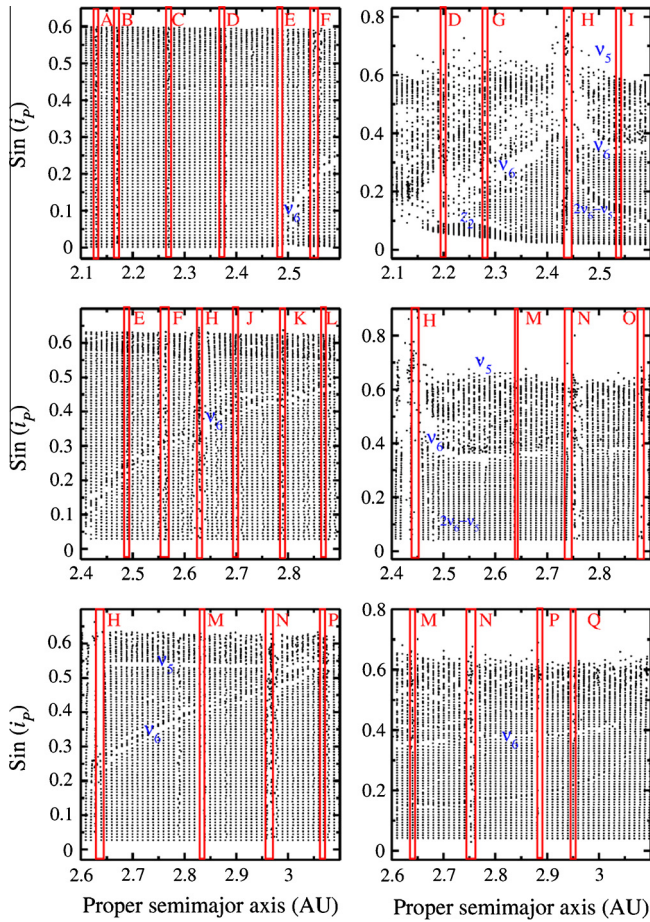


Fig. 3. Dynamical maps in proper $(a, \sin i)$ space for the planetary orbits in the jumping-Jupiter model, case_1, taken at $t = 0$ (left column), and $t = 10.0$ Myr (right column). The rows stand for the Vesta (top), Eunomia (middle), and Koronis (bottom) families. For each map, it was assumed a fixed initial eccentricity equal to the eccentricity of the representative body of the family. Blue labels identify the main secular resonances, and vertical red lines display the positions of the main mean motion resonances. These are named with a letter from A to Q, sequentially corresponding to the following resonances: 6j:–3S:1A, 8j:–2A, 5j:–2S:1A, 7j:2S:–1A, 2j:2S:–1A, 5j:–3S:1A & 5S:–1A, 5j:4S:–2A, 3j:–1A, 6j:–1S:2A, 1j:3S:–1A, 4j:–2S:1A, 2j:1S:1A, 8j:–3A, 5j:–2A, 7j:–3A, 3j:–1S:1A, and 9j:–4A. This is standard notation for 2-body and 3-body mean motion resonances, so pj:qS: kA stands for a resonance with critical frequency $pn_{\text{Jup}} + qn_{\text{Sat}} + kn_{\text{Ast}}$. (For interpretation of the references to color in this figure legend, the reader is referred to the web version of this article.)

dynamical maps for case_3 are very similar to the ones obtained for case_1.

The maps are obtained by computing synthetic proper elements in a grid of 51 by 81 (i.e., 4131) test particles in the $(a, \sin(i))$ plane, with fixed eccentricity. The proper elements are determined using the method discussed in Carruba (2010). Values of proper i ranged from 0° to 40° , while values of proper a were in the range from 2.1 to 2.6 AU (Vesta map), from 2.4 to 2.9 AU (Eunomia map), and from 2.6 to 3.1 AU (Koronis map), respectively. The eccentricity and other initial angles are fixed to the values of the corresponding parent body.

Results are shown in Fig. 3. Each black dot in these plots shows the proper elements of one test particle. Mean-motion resonances (hereafter MMRs), identified by vertical red lines in the figure, appear as vertical strips almost deprived of black points. Secular resonances appear as inclined bands also depleted of dots. We identify all MMRs up to order 13, and some linear and nonlinear secular resonances, in particular the ν_6 resonance, whose argument stands for $\varpi - \varpi_{\text{Sat}}$, and the z_1 resonance, whose argument stands

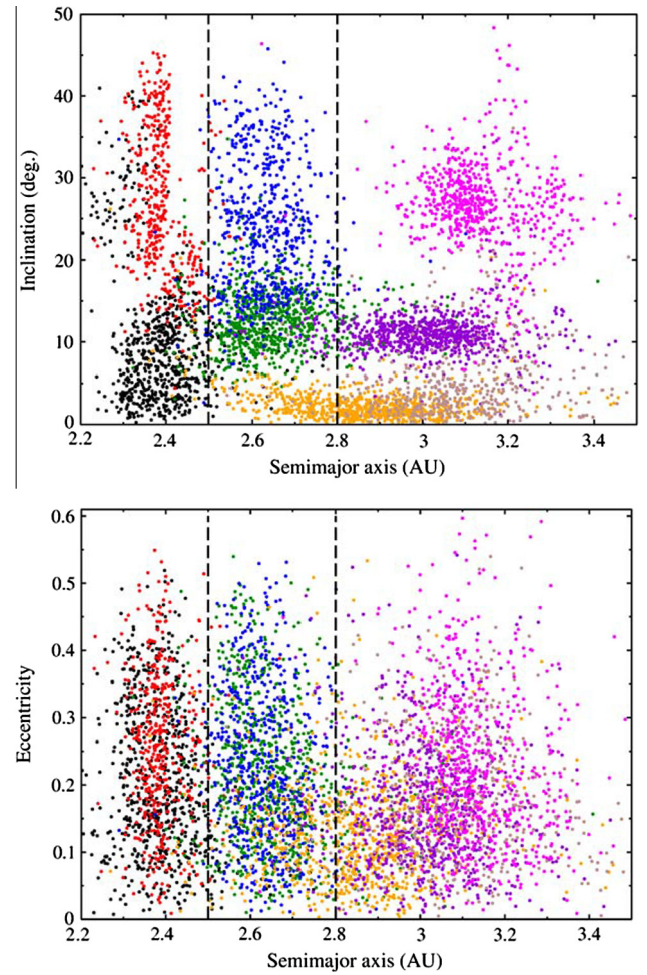


Fig. 4. The final orbital distribution of primordial, pre-LHB families for the case_1. The inclination with semimajor axis are shown in the upper panel, while the eccentricity with semimajor axis are shown in the bottom panel. The colors denote the fictitious families Vesta (black), Phocaea (red), Eunomia (green), Hansa (blue), Koronis (orange), Eos (violet), Themis (brown), and Euphrosyne (magenta). The dashed vertical lines stand for the approximate boundaries of the inner, central, and outer main belt regions. It can be noted that the families are strongly dispersed in all orbital elements. (For interpretation of the references to color in this figure legend, the reader is referred to the web version of this article.)

for $\varpi - \varpi_{\text{Sat}} + \Omega - \Omega_{\text{Sat}}$. The ν_{16} resonance, whose argument stands for $\Omega - \Omega_{\text{Sat}}$ does not appear in the dynamical maps, but as we will show later it plays a relevant role in the dynamics of the Vesta and Koronis families.

Fig. 3 shows that the position of the ν_6 secular resonance changes considerably between $t = 0$ and $t = 10$ Myr, crossing all the inner belt region, and parts of the central/outer belt as well. In the case of the Vesta map, the ν_6 resonance is initially at $a = 2.5$ AU for $i = 0$, and then evolves inwards over the Vesta family region during the instability. Also, the MMRs move significantly during the migration of Jupiter and Saturn. This fast resonance sweeping is expected to leave traces on the asteroid families. In Section 3.2, we present a detailed analysis of some of the most relevant mechanisms.

3. Results

In our simulations, we set the initial families as shown in Fig. 1 and evolve them under instability cases 1 and 3. The integrations last 10 Myr, and the instability occur at $t \simeq 5.72$ Myr in case_1, and $t \simeq 6.2$ Myr in case_3 (Fig. 2). The results are shown in Figs. 4

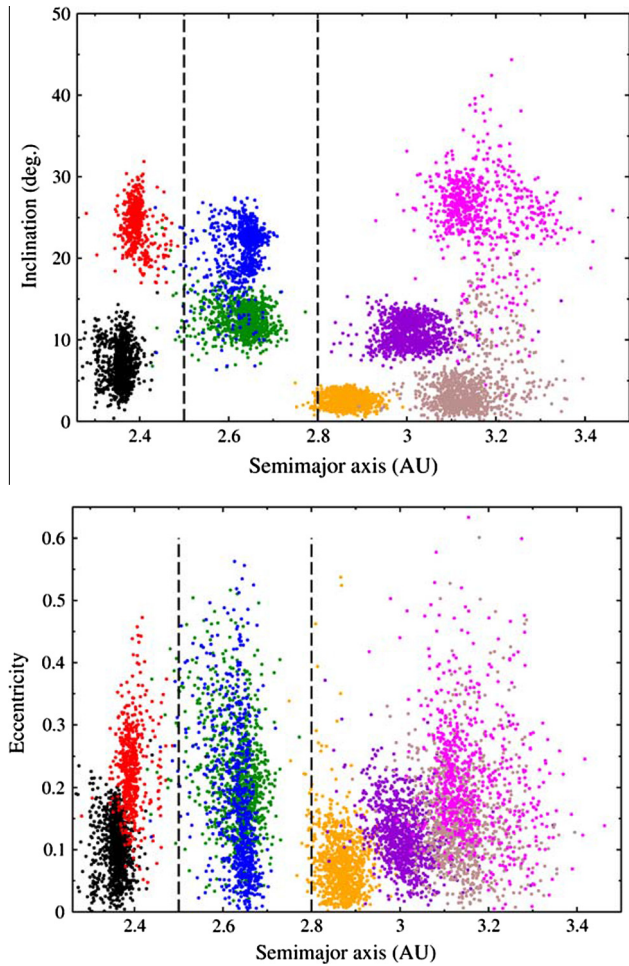


Fig. 5. Same as Fig. 4 for the case_3. Families are dispersed, especially in the eccentricity. However, the overall dispersion is not as strong as in case_1.

and 5. It is clear that most pre-LHB families do not survive the instability phase. They are considerably spread in semimajor axis, eccentricity, and inclination, specially in case_1. We also note that the high inclination families ($\sin i > 0.3$) appear to be much more dispersed, both in eccentricity and inclination, than the low inclination families. On the other hand, they are less dispersed in semimajor axis. It is worth stressing that these figures show osculating orbital elements. Although identification of asteroid families requires the computation of proper orbital elements, this is a time consuming procedure that is not necessary in the present case. Indeed, the families are so dispersed in the orbital space that proper and osculating elements would produce almost the same picture.²

Our results indicate that it is possible to disperse primordial families beyond recognition due to planetary perturbations, particularly in inclination. This is an important finding because the dispersed families could not be identified as compact clusters anymore, specially in case_1. In order to put this finding in evidence, we overlap the low inclination ($\sin i < 0.3$) families simulated in this study with the main belt background asteroids taken from Roig and Nesvorný (2015). The background was represented by ~6000–9000 objects such that the proportion of

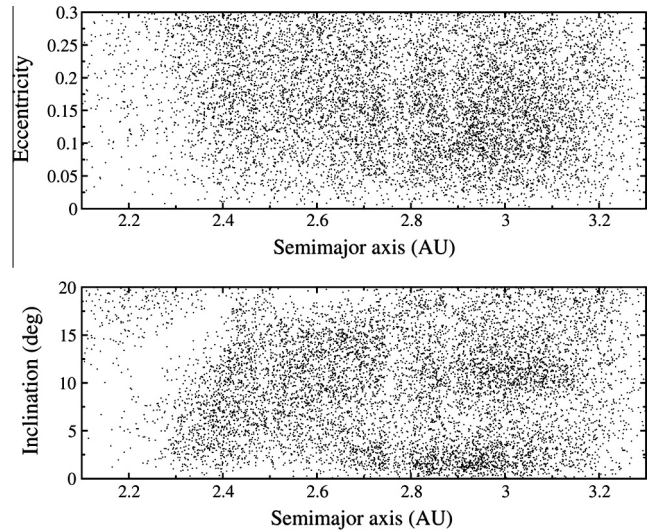


Fig. 6. Final eccentricity and semimajor axis (upper panel), and inclination and semimajor axis (lower panel) distributions for our five low- i (Vesta, Eunomia, Koronis, Themis, and Eos) families plus background asteroids for case_1.

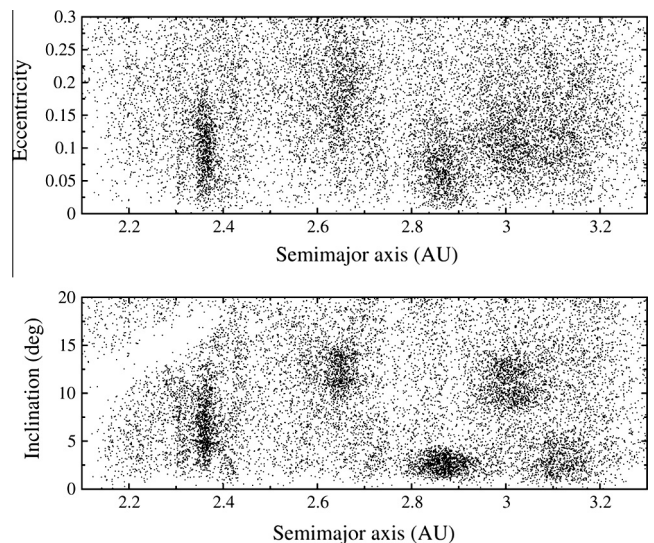


Fig. 7. The same as Fig. 6 for case_3.

background-to-family asteroids is roughly 2:1. This choice was motivated by the present population of asteroids with absolute magnitude $H < 12.7$ (diameter $D > 10$ km for albedo $p_v = 0.15$). This allows us to compare the distribution of the families to a background of asteroids obtained under identical simulation conditions. The result is shown in Figs. 6 (case_1) and 7 (case_3). We note that in case_1 the families cannot be distinguished from the background, and in case_3 some of them could be potentially recognized in inclination but not in eccentricity. This latter result is similar to the findings of Brož et al. (2013). The dispersal of families is stronger in case_1 than in case_3, partly because of the stronger effects of the interloper planet. In the following sections we will analyze the different effects that contribute to the dispersal. Finally, we note that if the comparison was done with fewer background asteroids, the dispersed asteroid families in case_1 would still not be identified, while chances to identify the families in case_3 would increase.

Results by Roig and Nesvorný (2015) indicate that after the jumping Jupiter instability, the asteroid belt suffers more

² It is worth recalling that the aspect of the dispersed families today would not look exactly like the ones presented in Figs. 4 and 5 because some of the dispersed asteroids fell on Mars crossing orbits, or have been affected by long term dynamical mechanisms.

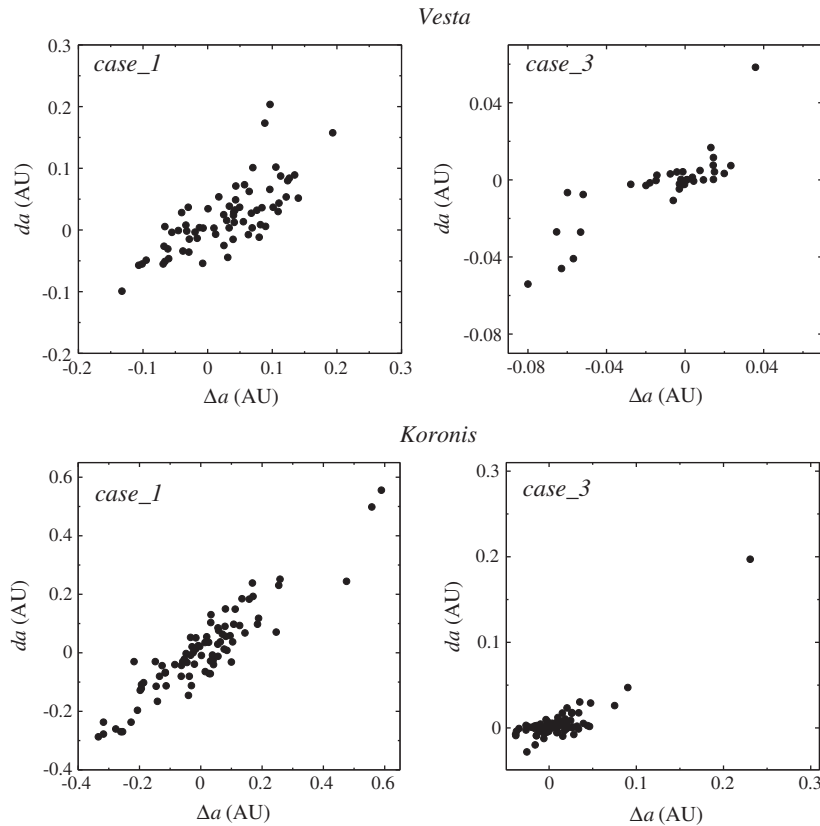


Fig. 8. Results of the semimajor axis displacement caused by the encounters with the interloper planet, da , and the total one, Δa . The rows show Vesta (upper) and Koronis (bottom) fictitious primordial families, while the columns stand for case_1 (left) and case_3 (right). There is a correlation between da and Δa in all plots, indicating that the fifth planet is indeed responsible for spreading the studied families in the semimajor axis.

dispersion, particularly during the ~ 100 Myr phase of residual smooth migration of the giant planets that follows the instability. This authors found that, for case_3, the average dispersion of the main belt after the instability is 0.07 AU in semimajor axis, 0.1 in eccentricity, and 3° in inclination. Therefore, one should expect a larger dispersion of our synthetic families than the one shown in Figs. 4 and 5.

3.1. Semimajor axis displacement

We looked into the effects of the interloper planet on the asteroidal orbital elements (a , e , i) adopting the following procedure. Each time any test particle had a close encounter – as defined in Section 2.3 – with the interloper planet, we compute the orbital displacement during the encounter interval as the difference between the heliocentric orbital elements before and after the particle evolves into/away from the sphere of influence of the planet (defined as 3 Hill radii). We thus obtain a complete data set with the changes in the a , e , i caused by all the close approaches of the particles with the interloper planet. Then, we calculate the overall changes for each particle by summing up the contribution of all encounters with that particle.

The correlation between the displacement in the semimajor axis caused by the encounters (da) and the total displacement (Δa) seen in the simulations is shown in Fig. 8. The correlation of da with Δa demonstrates that the encounters with the interloper planet are responsible for the total displacement in semimajor axis. Also, we note that case_1 is much more effective in spreading orbits relative to case_3 by one order of magnitude for Vesta, and at least by a factor of 2 for Koronis. Therefore, to summarize, we find that the hypothetical interloper planet could help to erase

the primordial asteroid families by dispersing them in the semimajor axis. An instability model without the interloper planet would instead lead to much better survival of the original clustering of the families in the semimajor axis (e.g. Brož et al., 2013).

As we showed in Figs. 4 and 5, both the eccentricities and inclinations are substantially dispersed during the instability, specially for case_1. In Fig. 9 we applied the same approach for these elements, as we have done for the semimajor axis. The figure shows the results for Vesta, in case_1. This time we observe no correlation between de and Δe , nor between di and Δi . This result is shared by all the other tested families in both instability cases. Thus, we can rule out the hypothetical fifth planet as the cause of the eccentricity and inclination spreading. A plausible mechanism of the eccentricity and inclination dispersal is discussed in the next section.

3.2. Eccentricity and inclination dispersal

Aiming to answer the question of which is/are the mechanism (s) responsible for spreading the eccentricities and inclinations of the particles, we have done a new set of simulations. Basically, the procedure is identical to the previous one, but we attribute zero mass to the interloper planet.³ This way we can single out the effects of the other giant planets, specially Jupiter and Saturn (although indirect perturbations of the interloper planet are still present in the simulation). It is clear from the dynamical maps shown in Section 2.4 that the ν_6 resonance crosses most the inner belt region, and also parts of the central and outer belt. Also, many low order MMRs with Jupiter and Saturn shift locations, due to the change in

³ It is worth noting that, since planetary coordinates are interpolated from previously stored orbits, this does not affect the evolution of the four giant planets.

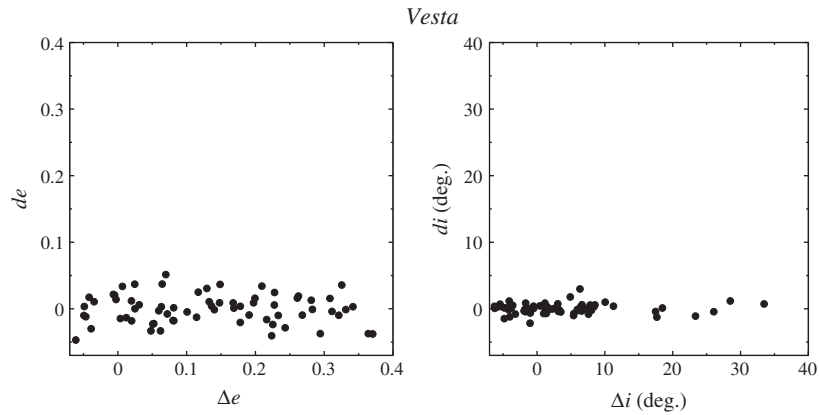


Fig. 9. Results of a simulation of case_1 for a Vesta-like family. Here we show that the effects of close encounters with the interloper planet (de and di) are small compared to the total change of these elements (Δe and Δi). The interloper planet therefore cannot be responsible for the total changes in the eccentricity and inclination.

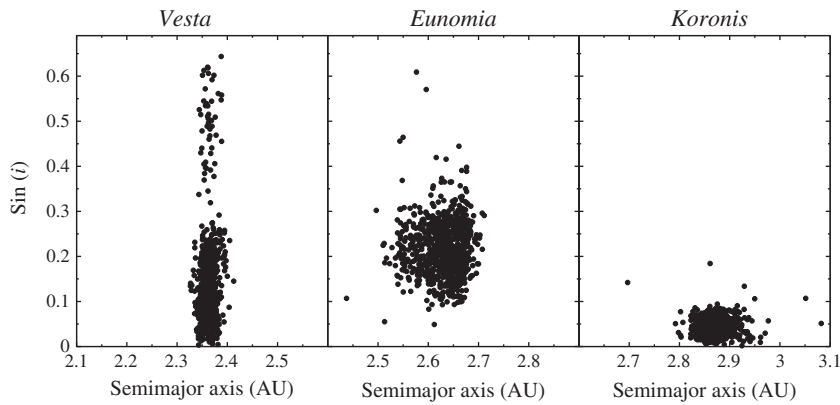


Fig. 10. Final $\sin i$ versus semimajor axis distribution, after 10 Myr, in case_1. The different panels show the Vesta (left), Eunomia (middle), and Koronis (right) families. The interloper planet is considered to have zero mass in these simulations. It is clear that other mechanism(s) than the direct perturbations of the fifth planet must be responsible for the inclination dispersal.

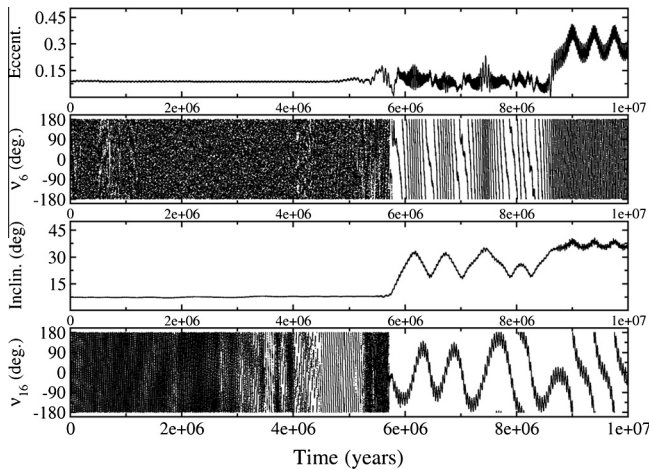


Fig. 11. Temporal evolution (from top to bottom) of eccentricity, the argument ($\varpi - \varpi_5$) of the v_6 resonance, inclination, and the argument ($\Omega - \Omega_5$) of the v_{16} resonance for a Vesta family particle, in case_1. The excitation in eccentricity and inclination are related to the evolution of the v_6 and v_{16} resonances, respectively.

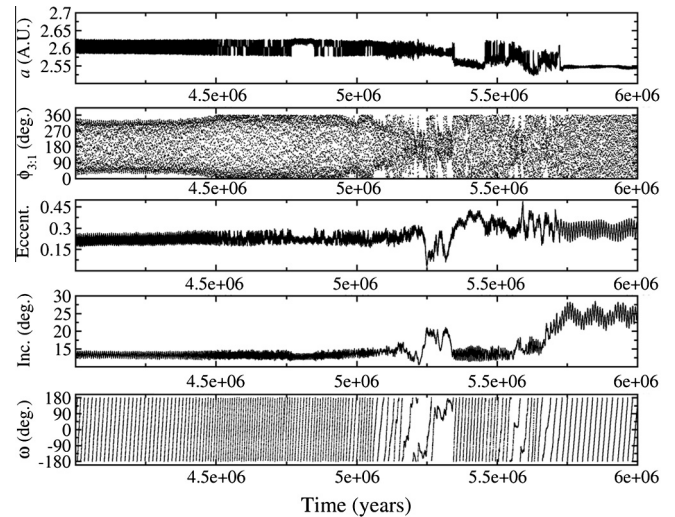


Fig. 12. Temporal evolution detail (from top to bottom) of semimajor axis, argument ($3\lambda_j - \lambda - 2\varpi$) of the 3:1 mean motion resonance (MMR), eccentricity, inclination, and argument of pericenter (ω) for a particle originally in the Eunomia family, in case_1. There is a capture into the 3:1 MMR followed by the Kozai resonance during the instability.

the semimajor axes of the gas giants during the instability. For example, the effect of the 2:1 MMR, which in our simulations ended at $a \simeq 3.2$ AU, is clearly noted in Figs. 4 and 5. In particular, it causes the large dispersion in (e, i) of the Euphrosyne family members. We also expect that other linear and nonlinear secular resonances that

cannot be seen in the dynamical maps of Fig. 3 affect the evolution, in particular the v_{16} resonance.

In Fig. 10, we show the final (at $t = 10$ Myr) inclination and semimajor axis of the Vesta, Eunomia, and Koronis families in a

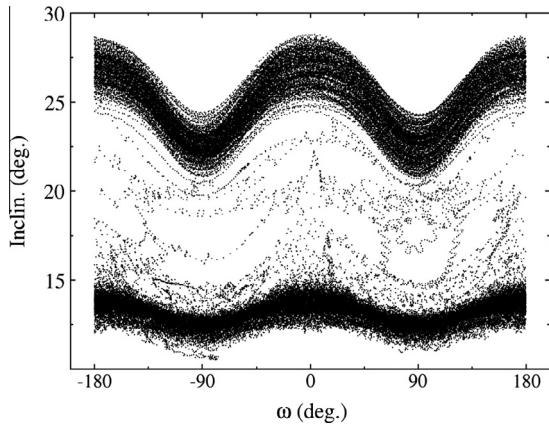


Fig. 13. Phase space (i, ω) of the same particle shown in Fig. 12, but for the whole integration interval (0–10 Myr). The islands around $\omega = -90^\circ$ and $\omega = 90^\circ$ are related to the Kozai resonance dynamics, which arises inside the 3:1 MMR during the instability phase.

simulation with zero mass of the interloper planet. These plots can be compared with the results presented in Fig. 4 and with the right column of Fig. 3. Since the fifth planet has zero mass in these simulations, the orbits roughly remain with the same semimajor axis they had originally (see Fig. 1). All the three families have their inclinations dispersed, and the dispersion seems to decrease for increasing semimajor axis. This is in line with the expectation from the behavior of the v_6 and v_{16} resonances discussed above. For example, we can infer from the dynamical maps that the Vesta family should have been crossed by the v_6 resonance. That dispersal effect is not as evident in the case of the Eunomia family, and is even smaller for the Koronis family, probably because the Koronis family has not suffered the v_6 and v_{16} resonance crossing.

By studying the temporal evolution of members of the Vesta family whose inclinations were raised up during the instability, it is possible to point out the actual effects of v_6 and v_{16} in more detail. Fig. 11 presents the temporal evolution of eccentricity, v_6 argument ($\varpi - \varpi_5$), inclination, and v_{16} argument ($\Omega - \Omega_5$) for a selected particle. Although the 7:2 MMR crosses the region of Vesta, no capture into this resonance was noted in the cases we

inspected. However, just at the time of the instability, the behavior of the argument of the v_6 resonance changes. This change is simultaneous to the excitation of the eccentricity. At the same time, the increase in inclination is related to the capture into the v_{16} resonance. This is a general trend for the Vesta family members that had the inclinations strongly excited.

We also noted a similar behavior for some Eunomia orbits reaching high inclinations, as shown in Fig. 12. The 3:1 MMR crosses the Eunomia family region (see Fig. 3). The particle shown in Fig. 12 is initially captured into this MMR and follows Jupiter's semimajor axis variation. Another secular effect, the Kozai resonance, is present during the instability phase, as noted by the libration of the argument of the pericenter (ω) and coupled variations of eccentricity and inclination. Even for small inclinations, the Kozai resonance can show up inside a mean motion resonance (Kozai, 1985; Gallardo et al., 2012). Fig. 13 presents the phase space (i, ω) in which is easy to note the Kozai dynamics that in this case occurs inside the 3:1 MMR.

3.2.1. Koronis case

The dispersion of the Koronis family appears to be related to more subtle mechanisms. In fact, we did not find any visible effect of the v_6 , nor of low-order mean motion resonances in our simulations. But the family has evidently suffered an (e, i) spreading, and this is clear when comparing Figs. 1 and 10. Thus, we have selected some particles that were dispersed in inclination and performed the simulations again, with an output step of 100 yr. In this way, we are able to look for other weaker resonances that also crossed the region during the instability.

Fig. 14 shows an illustrative case of what we have found for the Koronis-like members. We expect a similar behavior could be found in other low (e, i) primordial families. We focus on the interval starting just before the instability and ending 2 Myr after it. The particle is initially not captured in any resonance. But during the instability phase it becomes captured into the 5:2 MMR at $t \simeq 5.7$ Myr. Once inside the mean motion resonance, the dynamics changes and the particle is captured into secular resonances. In the case presented here, the v_5 and v_{16} resonances become active, raising the eccentricity and inclination, respectively. Additionally, we have found that the z_1 resonance is of great importance for the inclination dispersal. As shown by Knežević et al. (2002), this res-

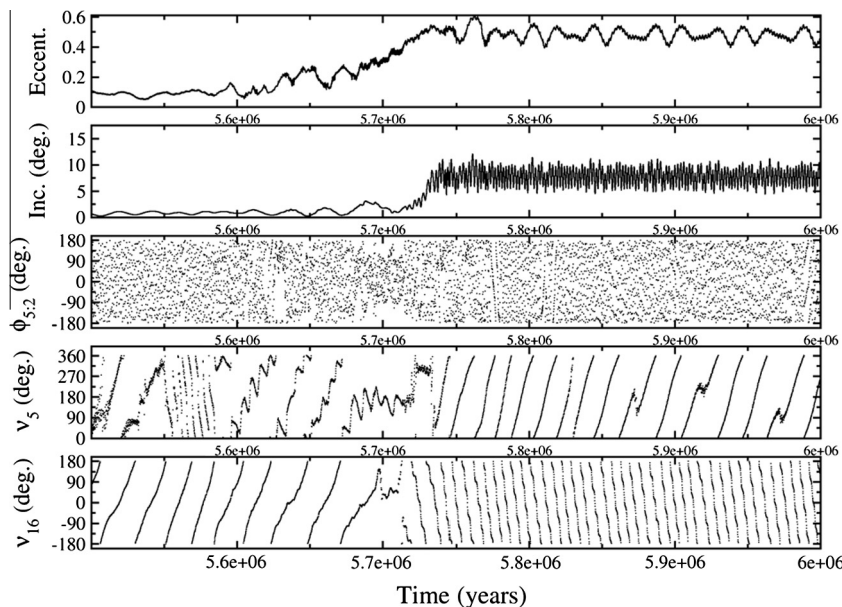


Fig. 14. Temporal evolution (from top to bottom) of eccentricity, inclination, resonant argument ($5j - 2\lambda - 3\varpi$) of the 5:2 MMR, the resonant argument ($\varpi - \varpi_j$) of the v_5 and v_{16} resonances, respectively, for a particle originating in Koronis family, in case_1. The overall increase in eccentricity and inclination is related to the captures in secular resonances while trapped in the MMR.

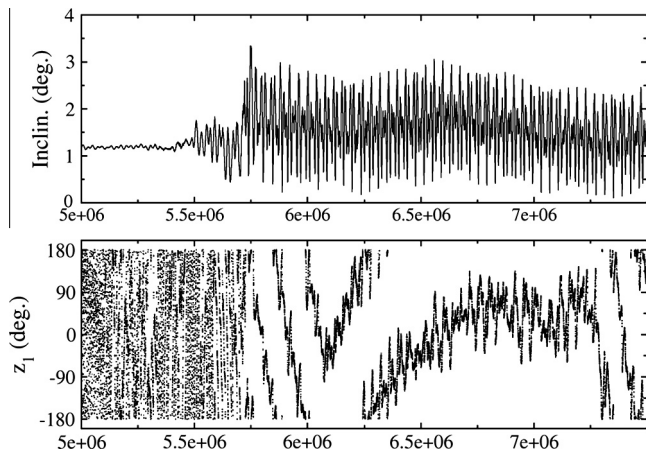


Fig. 15. Temporal evolution (from 5 to 7.5 Myr) of the inclination (top panel) and the argument ($\varpi - \varpi_6 + \Omega - \Omega_6$) of the z_1 resonance (lower panel), coming from a Koronis-like particle in the case_1. Despite it is not so strong as the other secular resonances, the z_1 can increase the amplitude of the inclination considerably.

onance currently lies close to the location of the Koronis family. Thus, it is expected that it moved away and have swept that region, causing the dispersal of the inclination of primordial asteroids that interacted with it. This effect, in fact, is observed for another Koronis-like particle shown by Fig. 15. Despite the effect of the z_1 resonance is not as strong as the ν_6 and ν_{16} resonances, it is sufficient to increase the inclination's amplitude of oscillation.

4. Conclusions

Here we studied the evolution of ancient (pre-LHB) asteroid families in the jumping-Jupiter model proposed by Nesvorný (2011), Nesvorný and Morbidelli (2012). This model assumes the initial presence of a fifth (interloper) giant planet in the outer Solar System that is ejected from the system after having encounters with Saturn and Jupiter. The results of this work are the following:

- Similarly to Brož et al. (2013), we show that due to the jumping-Jupiter instability, most primordial families disperse beyond recognition. However, our results indicate that planetary perturbations would be much more efficient in dispersing the families than was previously found by those authors. This is partly due to the fact that we are using a more realistic and accurate model of the instability than Brož et al. (2013).
- After being scattered into the asteroid belt region, the interloper planet has close encounters with the primordial asteroid family members. Those close encounters are responsible for spreading the semimajor axes of the family members, but not the eccentricities or inclinations.
- By overlapping the simulated families with background asteroids, the low- i families become unrecognizable, specially in case_1. The families can be potentially identified in inclination in case_3, although we expect that their detection using statistical methods like the Hierarchical Clustering Method would not be possible due to a significant spread in eccentricity. Since no old families are apparent in the inclination distribution of the present main belt, we suggest that the jumping-Jupiter evolutions resembling case_1 are preferred.
- During the instability phase, we note that many secular and MMRs with Jupiter and Saturn have crossed the asteroid belt. We find that the main linear secular resonances ν_6 and ν_{16} , some nonlinear secular resonances like the z_1 , and some secular resonances, like ν_5 and Kozai resonances inside the mean motion resonances, play the most important role in dispersing the inclination and eccentricity of the asteroid families.

- In general, the high inclination families are much more dispersed in eccentricity and inclination than the low inclination families, but less dispersed in semimajor axis. This latter is expected since the high inclination families have a lower encounter probability with the interloper planet.

Our main conclusion is that the jumping-Jupiter instability models are able to explain the current absence of primordial asteroid families while also satisfying many other Solar System constraints. However, not all jumping-Jupiter evolutions (e.g. Brož et al. (2013) and our case_3) are able to completely erase primordial families. This could be taken as evidence to favor the instability models resembling our case_1.

The scattering of the asteroid's semimajor axis caused by the close encounters with the interloper planet could contribute to the mixing of taxonomical classes in the main belt. In particular, the dispersion of a primordial Vesta-like family could be one possible source for the many V-type objects presently observed in the central and outer belt. This possibility is going to be discussed in more detail in a forthcoming paper.

Acknowledgments

We wish to thank M. Brož and an anonymous referee for their comments and suggestions that helped to improve the manuscript. This work has been supported by: (i) the Brazilian National Research Council (CNPq) through fellowship n° 312292/2013-9, grants n° 401905/2013-6, 305453/2011-4 and 166686/2014-0, within the Science Without Borders Program; (ii) NASA's Solar System Workings program; and (iii) the São Paulo State Science Foundation (FAPESP) through grant n° 14/06762-2. Simulations has made use of the computing facilities of the Laboratory of Astroinformatics (IAG/USP, NAT/Unicisul), supported by FAPESP grant n° 2009/54006-4 and INCT-A.

References

- Bottke Jr., W.F., 2002. The Effect of Yarkovsky Thermal Forces on the Dynamical Evolution of Asteroids and Meteoroids. In: Bottke, W.F., Jr. et al. (Eds.), *Asteroids III*. Univ. Arizona Press, pp. 395–408.
- Brasil, P.I.O., Nesvorný, D., Gomes, R., 2014. Dynamical implantation of objects in the kuiper belt. *Astron. J.* 148 id. 56.
- Brasser, R. et al., 2009. Constructing the secular architecture of the solar system II: the terrestrial planets. *Astron. Astrophys.* 507, 1053–1065.
- Brož, M. et al., 2013. Constraining the cometary flux through the asteroid belt during the late heavy bombardment. *Astron. Astrophys.* 551 id. A117.
- Carruba, V., 2010. The stable archipelago in the region of the Pallas and Hansa dynamical families. *Mon. Not. Roy. Astr. Soc.* 408, 580–600.
- Deienno, R. et al., 2014. Orbital perturbations of the Galilean satellites during planetary encounters. *Astron. J.* 148 id. 25.
- Dykhuis, M.J., Greenberg, R., 2015. Collisional family structure within the Nysa-Polana complex. *Icarus* 252, 199–211.
- Farinella, P. et al., 1993. The injection of asteroid fragments into resonances. *Icarus* 101, 174–187.
- Fernández, J.A., Ip, W.-H., 1984. Some dynamical aspects of the accretion of Uranus and Neptune - The exchange of orbital angular momentum with planetesimals. *Icarus* 58, 109–120.
- Gallardo, T., Gastón, H., Pais, P., 2012. Survey of Kozai dynamics beyond Neptune. *Icarus* 220, 392–403.
- Giblin, I. et al., 1998. The properties of fragments from catastrophic disruption events. *Icarus* 134, 77–112.
- Gomes, R. et al., 2005. Origin of the cataclysmic Late Heavy Bombardment period of the terrestrial planets. *Nature* 435, 466–469.
- Hahn, J.M., Malhotra, R., 1999. Orbital evolution of planets embedded in a planetesimal disk. *Astron. J.* 117, 3041–3053.
- Knežević, Z., Lemaître, A., Milani, A., 2002. The Determination of Asteroid Proper Elements. In: Bottke, W.F., Jr. et al. (Eds.), *Asteroids III*. Univ. Arizona Press, pp. 603–612.
- Kozai, Y., 1965. Secular perturbations of resonant asteroids. *Celest. Mech.* 36, 47–69.
- Levison, H.F. et al., 2008. Origin of the structure of the Kuiper belt during a dynamical instability in the orbits of Uranus and Neptune. *Icarus* 196, 258–273.
- Milani, A. et al., 2014. Asteroid families classification: Exploiting very large datasets. *Icarus* 239, 46–73.

- Minton, D., Malhotra, R., 2009. A record of planet migration in the main asteroid belt. *Nature* 457, 1109–1111.
- Morbidelli, A. et al., 1995. Asteroid families close to mean motion resonances: dynamical effects and physical implications. *Icarus* 118, 132–154.
- Morbidelli, A. et al., 2005. Chaotic capture of Jupiter's Trojan asteroids in the early Solar System. *Nature* 435, 462–465.
- Morbidelli, A. et al., 2009. Constructing the secular architecture of the solar system. I. The giant planets. *Astron. Astrophys.* 507, 1041–1052.
- Morbidelli, A. et al., 2010. Evidence from the asteroid belt for a violent past evolution of Jupiter's orbit. *Astron. J.* 140, 1391–1401.
- Nesvorný, D., 2011. Young Solar System's Fifth Giant Planet? *Astrophys. J.* 742 id. L22.
- Nesvorný, D., 2015. Jumping Neptune can explain the kuiper belt kernel. *Astron. J.* 150 id. 68.
- Nesvorný, D., Morbidelli, A., 2012. Statistical study of the early solar system's instability with four, five, and six giant planets. *Astron. J.* 144 id. 117.
- Nesvorný, D., Vokrouhlický, D., Morbidelli, A., 2013. Capture of trojans by jumping Jupiter. *Astrophys. J.* 768 id. 45.
- Nesvorný, D., Vokrouhlický, D., Deienno, R., 2014a. Capture of irregular satellites at Jupiter. *Astrophys. J.* 784 id. 22.
- Nesvorný, D. et al., 2014b. Excitation of the orbital inclination of iapetus during planetary encounters. *Astron. J.* 148 id. 52.
- Nesvorný, D., Brož, M., Carruba, V., 2015. Identification and Dynamical Properties of Asteroid Families. In: Michel, P., De Meo, F.E., Bottke, W.F., Jr. (Eds.), *Asteroid IV*. Univ. Arizona Press and LPI (in press).
- Petit, J.-M., Farinella, P., 1993. Modelling the outcomes of high-velocity impacts between small solar system bodies. *Cel. Mech. Dyn. Astr.* 57, 1–28.
- Roig, F., Nesvorný, D., 2015. The evolution of Asteroids in the jumping-Jupiter migration model. *Astron. J.* 150 id. 186.
- Spoto, F., Milani, A., Knežević, Z., 2015. Asteroid family ages. *Icarus* 257, 275–289.
- Tsiganis, K. et al., 2005. Origin of the orbital architecture of the giant planets of the solar system. *Nature* 435, 459–461.